Tomographic Reconstruction of Piecewise Smooth Images

Christopher V. Alvino   Anthony J. Yezzi, Jr.

School of Electrical and Computer Engineering
Georgia Institute of Technology
Atlanta GA, 30332
alvino@ece.gatech.edu   ayezzi@ece.gatech.edu

Abstract

In computed tomography, direct inversion of the Radon transform requires more projections than are practical due to constraints in scan time and image accessibility. Therefore, it is necessary to consider the estimation of reconstructed images when the problem is under-constrained, i.e., when a unique solution does not exist. To resolve ambiguities among solutions, it is necessary to place additional constraints on the reconstructed image. In this paper, we present a surface evolution technique to model the reconstructed image as piecewise smooth. We model the reconstructed image as two regions that are each smoothly varying in intensity and are separated by a smooth surface. We define a cost functional to penalize deviation from piecewise smoothness while ensuring that the projections of the estimated image match the measured projections. From this functional, we derive an evolution for the modeled image intensity and an evolution for the surface, thereby defining a variational tomographic estimation technique. We show example reconstructions to highlight the performance of the proposed method on real medical images.

1. Introduction

In computed tomography, the goal is to reconstruct an image from its measured projections that are modeled by the Radon transform. While it is possible to invert the Radon transform in theory [1], in practice it requires a large amount of projection data to obtain a high-quality reconstruction. For a review of tomographic reconstruction methods, we refer the reader to [2]. Constraints in cost, scan time, and image accessibility limit the number and quality of projections. Therefore, it is often not feasible in practice to obtain the amount of projections necessary to reconstruct accurately. For this reason, several authors have considered solving the under-constrained or *limited-angle* tomographic reconstruction problem [3, 4, 5, 6, 7].

Additional assumptions must be made about the image function to properly constrain the possible solutions. Au-
thors have attempted different constraints depending on the assumptions they wish to make about the unknown images. Sezan and Stark use projection onto convex sets (POCS) to incorporate priors [4]. Reeds and Shepp use a technique called "squashing" to effectively add additional constraints [5]. Prince and Willsky introduce a smoothing procedure by using Markov random fields [6].

We will concentrate on a class of image priors that were addressed by Mumford and Shah's pioneering work on region-based image segmentation [8]. That is, we wish to consider the class of piecewise constant or, more generally, piecewise smooth images. Mumford and Shah considered segmenting images by assuming piecewise smooth regions separated by deformable or "active" contours, across which smoothness is not required. Chan and Vese [9] incorporated these ideas into the level set framework introduced by Osher and Sethian [10], allowing the contours to naturally handle topology changes. Active contour models are attractive because they are both well-principled and robust. Since Mumford and Shah's work, several ideas have emerged to make use of active contour models. [11, 12, 13].

In tomographic reconstruction, three major works have been presented that make use of active contour models. Yu and Fessler presented an early discrete approach to solve this problem [14]. They defined a discrete cost functional to model the reconstruction by an image partitioned into two regions separated by a deformable discrete boundary analogous to the contour proposed by Mumford and Shah. However, Yu's method for maintaining a smooth surface depends on the accuracy of the image estimate. This accuracy can not be guaranteed upon the initialization of the algorithm. In fact, they ignore this term in their implementation.

Bruandet et al. have proposed a surface evolution technique to model the reconstructed image as two regions, one with density zero, and the other with an *a priori* known density, μ [15]. Whitaker and Elangovan have proposed a similar, although slightly more general, piecewise constant model where the two region densities are adaptive [16]. The models of Bruandet and Whitaker are adequate when the regions being imaged are known to be homogeneous

in density, but this may not be the case in practice. Images often have smoothly varying densities, and often have three or more distinct regions. For this reason, it is desirable to generalize the piecewise constant models of Bruandet and Whitaker. By allowing the intensity of each pixel to vary independently, while enforcing that within regions, nearby pixels have similar intensities, we can successfully constrain the reconstructed image to be piecewise smooth.

In this paper, we define an deformable surface model to constrain tomographic images to be piecewise smooth. We propose a functional that attains a high value when the projections of the estimated reconstruction deviate from the measured projections, and attains a high value when the reconstructed image deviates from piecewise smoothness. By deforming the image model parameters to minimize this functional, we ensure that the reconstructed image matches the measured projections and is piecewise smooth.

2. Tomography Model

Although easily generalized to higher dimensions, we will describe the tomography problem in two dimensions, i.e., with two-dimensional image functions and one-dimensional projections. The reconstruction technique developed in this paper holds for the three-dimensional problem. Displaying the mathematical explanation and simulation results in two dimensions allows the authors to explain the technique more clearly.

Unknown image density function, $f : \mathbb{R}^2 \to \mathbb{R}$, will, via the Radon transform, create projections,

$$p(s, \theta) = \int_\Omega f(x, y) \delta(P_\theta(x, y) - s) d\bar{x}, \qquad (1)$$

where $P_\theta(x, y) = x \cos\theta + y \sin\theta$, and $d\bar{x}$ stands for integration in the spatial variables x and y.

The tomographic reconstruction problem is that of obtaining an estimate of f, which we will denote $\hat{f}$, from P projections $p(s, \theta_1), \ldots, p(s, \theta_P)$.

3. Proposed Reconstruction Method

In order to determine the shape of the contour that separates the piecewise smooth regions, we impose a cost on the discrepancy between the projections of the estimated image and the measured projections. However, since the problem is under-constrained, imposing this cost is not enough. Many images that are not piecewise smooth will also match the measured projections.

Therefore, we impose a cost on the deviation of the reconstructed image from piecewise smoothness. Properly enforcing piecewise smoothness requires penalizing two separate undesirable features of the model. Piecewise smoothness implies that large gradients in image intensity

within regions should be penalized. In addition, total contour length should also be penalized, for otherwise, the contour could converge to an irregular shape to match image noise.

3.1 Piecewise Smooth Cost Functional

We propose a cost functional that has three terms: the projection matching term, J_1; the function smoothness term, J_2; and the contour length term J_3. We combine these terms with weighting parameters to obtain the overall cost functional $J = \alpha J_1 + \beta J_2 + \gamma J_3$, where,

$$J_1 = \sum_{\theta \in \Theta} \int_0^{L_\theta} (p(s, \theta) - \hat{p}(s, \theta))^2 \, ds, \qquad (2)$$

$$J_2 = \int_{R_1} \|\nabla \hat{f}_{R_1}(x, y)\|^2 d\bar{x} + \int_{R_2} \|\nabla \hat{f}_{R_2}(x, y)\|^2 d\bar{x}, \quad (3)$$

$$J_3 = \int_0^L d\ell. \qquad (4)$$

Note that $\Theta = \{\theta_1, \ldots, \theta_P\}$ is the set of projection angles, L_θ is the length of the projection at angle θ. Also, $\hat{p}(s, \theta)$ is the Radon transform of the image estimate $\hat{f}$. The symbol ∇ is the standard gradient operator.

In J_2, note that the function $\hat{f}$ has been split into two open regions, R_1 and R_2, that are subsets of the image domain. These are regions where $\hat{f}$ is guaranteed to be differentiable. We will denote the restriction of $\hat{f}$ to region R_i as $\hat{f}_{R_i}$. The reason for this function restriction is that the piecewise smooth model can not guarantee differentiability on the contour, $\partial R = \partial R_1 = \partial R_2$, that separates the two regions. Thus, any attempt to differentiate on the boundary, ∂R, would be poorly defined. Finally, L is the length of the contour and $d\ell$ is the arc length element of the contour.

3.2 Evolution Equations

By introducing an evolution time parameter, t, into the image intensity functions and into the contour, we now have a cost functional that is dependent on t. Differentiating the three terms in the cost functional, J, with respect to t, we obtain,

$$\frac{dJ_1}{dt} = \int_0^L \left\langle \vec{C}_t, \left(\hat{f}_{R_1} - \hat{f}_{R_2} \right) \times \qquad (5)$$

$$\sum_{\theta \in \Theta} (\hat{p} - p) (P_\theta(x, y), \theta) \, \vec{n}_{R_1} \right\rangle d\ell$$

$$+ \int_{R_1} \hat{f}_{R_1, t} \sum_{\theta \in \Theta} (\hat{p} - p) (P_\theta(x, y), \theta) d\bar{x}$$

$$+ \int_{R_2} \hat{f}_{R_2, t} \sum_{\theta \in \Theta} (\hat{p} - p) (P_\theta(x, y), \theta) d\bar{x}$$

$$\frac{dJ_2}{dt} = \int_0^L \left\langle \vec{C}_t, \left(\|\nabla \hat{f}_{R_1}\|^2 - \|\nabla \hat{f}_{R_2}\|^2 \right) \vec{\nu}_{R_1} \right\rangle d\ell \quad (6)$$

$$+ \int_{R_1} \hat{f}_{R_1,t} \Delta \hat{f}_{R_1} d\bar{x}$$

$$+ \int_{R_2} \hat{f}_{R_2,t} \Delta \hat{f}_{R_2} d\bar{x},$$

$$\frac{dJ_3}{dt} = \int_0^L \left\langle \vec{C}_t, \kappa \nu \vec{R}_1 \right\rangle d\ell \quad (7)$$

where $\vec{C}_t$ is the partial derivative of the contour with respect to time, $\langle \cdot \rangle$ denotes the two-dimensional Euclidean dot product, Δ represents the Laplacian operator, and κ is the curvature of the contour. Also, $\hat{f}_{R_1,t}$ and $\hat{f}_{R_2,t}$ are partial derivative of the two image functions with respect to time. The unit normal vector at each point in the contour that points from region R_1 to region R_2 is denoted as $\vec{\nu}_{R_1}$.

The detailed derivations of Eqs. (5), (6), and (7) make use of the divergence theorem, but are omitted for brevity. We would like to point out that a factor of two is left out because it appears in all three equations. In the evolution implementation, this is equivalent to evolving the contours and image functions at half the speed.

By evolving the contour and image intensity functions to make Eqs. (5), (6), and (7) negative, we ensure that the cost functional is decreasing. This is achieved by evolving both the contour and image intensity functions in the directions opposite to the terms by which they are multiplied in Eqs. (5), (6), and (7). For instance, Eq. (5) tells us that by setting evolution of the contour to,

$$\vec{C}_t = - \left(\hat{f}_{R_1} - \hat{f}_{R_2} \right) (\vec{C}) \sum_{\theta \in \Theta} (\hat{p} - p) \left(P_\theta(x,y), \theta \right) \vec{\nu}_{R_1},$$
$$(8)$$

we guarantee that the first term in Eq. (5) will be negative. Hence, this term in Eq. (5) will then contribute to a decrease in total energy. In this manner, and by the linearity of differentiation, we obtain that the evolution equations that will minimize the proposed cost functional are,

$$\vec{C}_t = -\alpha \left(\hat{f}_{R_1} - \hat{f}_{R_2} \right) \sum_{\theta \in \Theta} (\hat{p} - p) \left(P_\theta(x,y), \theta \right) \vec{\nu}_{R_1} \quad (9)$$

$$-\beta \left(\|\nabla \hat{f}_{R_1}\|^2 - \|\nabla \hat{f}_{R_2}\|^2 \right) \vec{\nu}_{R_1}$$

$$-\gamma \kappa \nu \vec{R}_1$$

$$\hat{f}_{R_1,t} = -\alpha \sum_{\theta \in \Theta} (\hat{p} - p) \left(P_\theta(x,y), \theta \right) \quad (10)$$

$$-\beta \Delta \hat{f}_{R_1}$$

$$\hat{f}_{R_2,t} = -\alpha \sum_{\theta \in \Theta} (\hat{p} - p) \left(P_\theta(x,y), \theta \right) \quad (11)$$

$$-\beta \Delta \hat{f}_{R_2}.$$

4. Implementation

We implement Eqs. (9), (10), and (11) in a two-step iterative algorithm. The first step of the algorithm is to evolve the image intensity functions by Eqs. (10) and (11) until they are converged. This step is performed while holding the contour fixed. The second step of the algorithm is to evolve the contour by one forward time step of Eq. (9). We iterate these two steps until the contour no longer moves; at this point the algorithm is considered to be converged.

Note that, although the evolution equations are continuous both spatially and temporally (evolution being time), the algorithm has been implemented discretely. Thus, all image derivatives have been approximated by appropriate finite differencing schemes. Likewise, the evolution steps have been approximated by the standard forward Euler scheme.

In addition, it is important to note that, while image derivatives within regions are well-defined, image derivatives do not exist on the boundaries of the image or on the contour separating the two regions. We have assumed Neumann boundary conditions to handle these cases, i.e., at the boundaries, the directional derivatives of the functions in the directions normal to the boundaries are zero.

4.1 Image Intensity Evolution

We will briefly discuss the implementation of each of the evolution equations. Eqs. (10) and (11) are implemented by updating the image intensity functions, $\hat{f}_{R_1}$ and $\hat{f}_{R_2}$, by the forward Euler scheme, i.e.,

$$\hat{f}_{R_1}^{n+1} = \hat{f}_{R_1}^n + \Delta t \hat{f}_{R_1,t}^n \quad (12)$$

$$\hat{f}_{R_2}^{n+1} = \hat{f}_{R_2}^n + \Delta t \hat{f}_{R_2,t}^n, \quad (13)$$

where the superscript n denotes iteration number and Δt is the iteration time step parameter. This time step parameter is chosen to ensure stability of the algorithm. Note that the evolutions, $\hat{f}_{R_1,t}^n$ and $\hat{f}_{R_2,t}^n$, depend on the reconstruction estimates, $\hat{p}$, and thus is it required to update the projections each time these updates are performed. In this manner, we have update equations that minimize the cost functional, thereby ensuring both smoothness of the reconstruction and that the reconstruction projections match the measured projections.

4.2 Contour Evolution

We represent the contour in our model using level set techniques. That is, the contour is the set of points in the image domain where some level set function, Ψ, equals a chosen constant. Level set techniques implicitly represent the contour and thus have the ability to naturally handle topology changes while avoiding cumbersome and numerically unstable parameterizations.
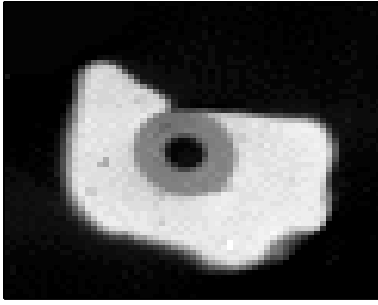
COMPUTER
SOCIETY

Figure 1: True 71×71-pixel bone image.

We evolve the level set function by,

$$\frac{d\Psi}{dt} = -\vec{C}_t \|\nabla \Psi\|^2 , \qquad (14)$$

which guarantees that the contour of interest moves according to the evolution given by Eq. (9). In fact, for computational efficiency, we only evolve the level set function, Ψ, in a thin band near the contour. After each level set function evolution step, we reinitialize the level set function to preserve distance. This reinitialization maintains a numerically well-behaved level set function.

5. Simulations

Before we present simulation results, we would like to make a note concerning the choices of the weight parameters α, β, and γ. We have achieved the simulation results in this paper by only scaling these parameters to account for differences in image size. Thus, the proposed method does not require significant fine tuning to achieve the results shown.

5.1 Bone Reconstruction

In Fig. 1 we show a 71×71-pixel grayscale image that is a cross-section of a piece of bone. This image is nearly piecewise constant. However, unlike the technique presented by Whitaker that models only two image regions, this bone image has three distinct intensity regions. For this reason, it is desirable to consider the three regions separately.

In Fig. 2 we show several stages of evolution of the proposed method. The top left image shows the initialization of the algorithm, where the image domain is subdivided into a large number of densely-spaced separate regions. The evolution of the algorithm proceeds from left to right in the top row and then is continued on the bottom row where it again proceeds left to right. The final reconstruction is show on the bottom right. Note how the three distinct homogeneous regions are accurately captured by the proposed model.

We compare the proposed method with the reconstruction from other techniques in Fig. 3. All reconstructions in this figure have used 9 equally-spaced projections. In
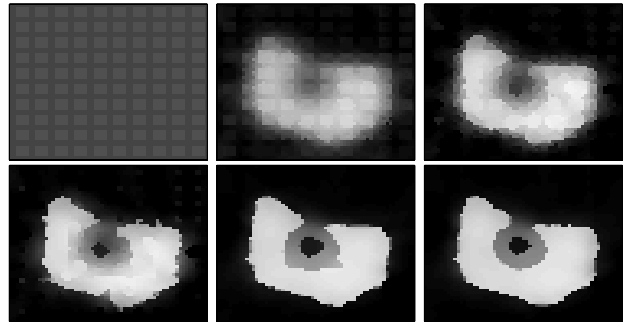

Figure 2: Several stages of bone reconstruction from 9 equally-spaced projections using proposed method. Algorithm initialization in top left image. Evolution proceeds from left to right and is continued in the second row. Final reconstruction on bottom right.

the top left, we show the true image for comparison. On the top right, we show the reconstruction using filtered back projection (FBP). On the bottom left, we display the reconstruction using the piecewise constant method proposed by Whitaker. On the bottom right, we show the reconstruction obtained from the proposed method.

Note that the proposed method most accurately represents the delineation between foreground and background. The reconstruction from FBP contains significant streak noise, as typically occurs with under-constrained FBP. The reconstruction from the piecewise constant model does not accurately represent the bone marrow region that lies inside of the bone. This occurs because the piecewise constant model is unable to represent more than two grayscale intensities.

5.2 Brain Reconstruction

In Fig. 4 we show a 145×145-pixel grayscale image that is a cross-section of a human skull and brain. This image has significant piecewise smooth structure, the boundaries between the bone and the gray matter have large intensity variation, but within the bone gray matter regions, the image has significant smoothness.

We show, in Fig. 5, several stages of the brain reconstruction using the proposed method. In this reconstruction we used 25 equally-spaced projections. Again, in the top left, we show the initialization of the algorithm with densely-spaced separate square regions. The algorithm proceeds from left to right. Notice how accurately the edges of the skull region are segmented by the contour in the proposed model.

In Fig. 6, we compare the brain reconstruction with the reconstruction from other methods. All methods in this comparison used 25 equally-spaced projections. In the top left we show the true brain CT image. In the top right
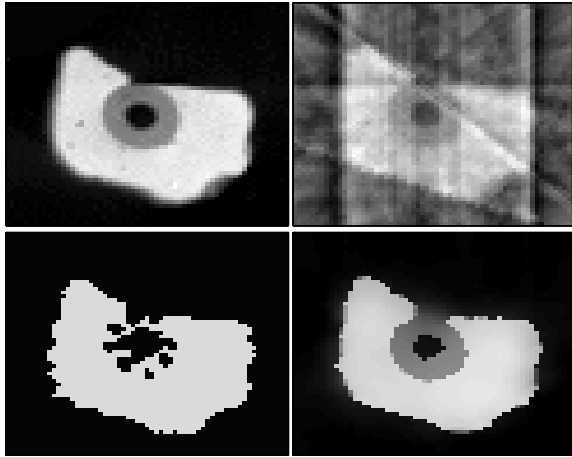
Figure 3: Comparison of bone reconstruction methods from 9 equally-spaced projections. True image (top left), filtered back projection reconstruction (FBP) (top right), piecewise constant reconstruction (bottom left), and proposed piecewise smooth reconstruction (bottom right).

Figure 4: True 145×145-pixel brain CT image (courtesy of the Department of Medical Imaging and Radiation Sciences at Monash University.)

we show the reconstruction using filtered back projection (FBP). In the bottom left, we show the reconstruction using the piecewise constant model and in the bottom right we show the reconstruction using the proposed piecewise smooth model.

Again note the accuracy with which the proposed model segments some of the small scale features of the skull and brain. The piecewise constant model attempts to represent the medium-intensity gray matter inside the skull region by considering part of the region to be foreground and part of the region to be background. The segmentation produced by the proposed model more accurately represents the physical boundaries between anatomical regions.
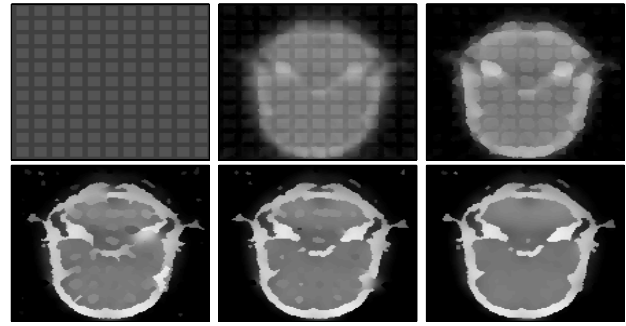

Figure 5: Several stages of brain reconstruction from 25 equally-spaced projections using proposed method. Algorithm initialization in top left image. Evolution proceeds from left to right and is continued in the second row. Final reconstruction on bottom right.

6. Discussion

We have presented a technique for reconstruction of tomographic images from Radon transform projections that explicitly deals with the under-constrained nature of the limited-angle tomography problem by enforcing priors on the reconstructed image. The technique, in addition to accurately reconstructing images, also separates the image into regions, thereby segmenting the image. Segmenting the reconstructions of the methods that have been compared against would produce inferior results to the segmentations obtained directly from this model. In limited-angle tomography filtered back projection produces reconstructions that are streaky and hence difficult to segment. Piecewise constant reconstruction produces segmentations but they are inaccurate when the image is not piecewise constant.

Although the presented results have been explicitly for two dimensions, the technique is easily generalized to three-dimensional image functions. Much of the discussion remains the same, however, in three dimensions, a surface represents the boundary between regions instead of a contour. The resulting evolution equations for the three-dimensional problem are obvious three-dimensional generalizations of the evolution equations proposed in this paper. The curvature term in Eq. (7) for the contour embedded in two dimensions becomes mean curvature for the surface in three dimensions. The authors are in the process of implementing the proposed technique in three dimensions.

The computational requirements of this technique are much higher than that of filtered back projection and significantly higher than that of piecewise constant reconstructions due to the evolution of the image intensity functions. For future work for this technique we suggest solving for the intensity of the image regions using multigrid techniques to achieve higher computational efficiency.

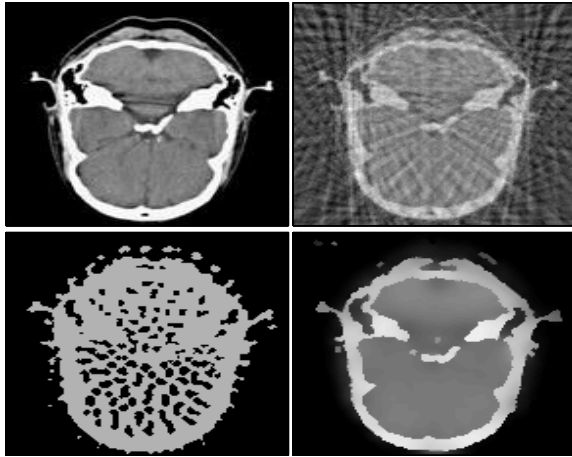In this paper, we have made little discussion about the

Figure 6: Comparison of brain reconstruction methods from 25 equally-spaced projections. True image (top left), filtered back projection reconstruction (FBP) (top right), piecewise constant reconstruction (bottom left), and proposed piecewise smooth reconstruction (bottom right).

type of initial contour. In our simulations, we initialized with a densely-spaced group of squares that spans the entire image. Other authors use a thresholded version of the reconstruction that has minimum norm or a thresholded version of the filtered back projection reconstruction [15, 16].

Acknowledgments

References

[1] S. Helgason, *The Radon Transform*, Springer Verlag, 1999.

[2] A. G. Ramm and A. I. Katsevich, *The Radon Transform and Local Tomography*, CRC Press Inc., Boca Raton, FL, 1996.

[3] T. Inouye, "Image reconstruction with limited angle projection data," *IEEE Transactions on Nuclear Science*, vol. 26, pp. 2666–2684, 1979.

[4] M. I. Sezan and H. Stark, "Tomographic image reconstruction from incomplete view data by convex projections and direct fourier inversion," *IEEE Trans. on Med. Imaging*, vol. 3, pp. 91–98, 1984.

[5] J. A. Reeds and L. A. Shepp, "Limited angle reconstruction in tomography via squashing," *IEEE Trans. on Med. Imaging*, vol. 6, pp. 89–97, June 1987.

[6] J. L. Prince and A. S. Willsky, "Hierarchical reconstruction using geometry and sinogram restoration," *IEEE Trans. on Image Proc.*, vol. 2, no. 3, pp. 401–416, July 1993.

[7] N. Robert, F. Peyrin, and M. Yaffe, "Binary reconstruction from a limited number of cone beam projections," *Medical Physics*, vol. 21, no. 12, pp. 1839–1851, 1994.

[8] D. Mumford and J. Shah, "Optimal approximation by piecewise smooth functions and associated variational problems," *Comm. Pure Appl. Math.*, vol. 17, pp. 577–685, 1989.

[9] T. F. Chan and L. A. Vese, "A level set algorithm for minimizing the Mumford-Shah functional in image processing," Tech. Rep. CAM 00-13, UCLA, Department of Mathematics, 2000.

[10] S. Osher and J. Sethian, "Fronts propagating with curvature-dependent speed: algorithms based on the Hamilton-Jacobi equations," *Journal of Computational Physics*, vol. 79, pp. 12–49, 1988.

[11] V. Caselles, R. Kimmel, and G. Sapiro, "Geodesic active contours," in *Proceedings of the IEEE Int. Conf. on Computer Vision*, Cambridge, MA, USA, June 1995, pp. 694–699.

[12] M. Kass, A. Witkin, and D. Terzopolous, "Snakes: Active contour models," *Int. Journal of Computer Vision*, vol. 1, pp. 321–331, 1987.

[13] S. Zhu and A. Yuille, "Region competition: Unifying snakes, region growing, and bayes/MDL for multi-band image segmentation," *IEEE Trans. on Pattern Analysis and Machine Intelligence*, vol. 18, no. 9, pp. 884–900, 1996.

[14] D. Yu and J. Fessler, "Edge-preserving tomographic reconstruction with nonlocal regularization," in *Proceedings of IEEE Int. Conf. on Image Proc.*, Chicago, IL, USA, Oct. 1998, vol. 1, pp. 29–33.

[15] J.-P. Bruandet, F. Peyrin, J.-M. Dinten, and M. Barlaud, "3D tomographic reconstruction of binary images from cone beam projections: A fast level set approach," in *IEEE Symposium on Biomedical Imaging*, Washington, D.C., July 2002, pp. 677–80.

[16] R. Whitaker and V. Elangovan, "A direct approach to estimating surfaces in tomographic data," *Journal of Medical Image Analysis*, vol. 6, no. 3, pp. 235–249, 2002.